

Hindered surface diffusion of bonded molecular clusters mediated by surface defects

William S. Huxter^{1,*}, Chandra Veer Singh^{1,2}, Jun Nogami^{1,†}

¹ Department of Materials Science and Engineering, University of Toronto, 184 College St., Toronto, ON M5S 3E4, Canada

² Department of Mechanical and Industrial Engineering, University of Toronto, 5 King's College Road, Toronto, Ontario, M5S 3G8, Canada

* Present address: Department of Physics, ETH Zurich, Otto Stern Weg 1, 8093 Zurich, Switzerland

† Corresponding Author: jun.nogami@utoronto.ca

ABSTRACT

We reveal how substrate surface defects hinder the mobility of sub-monolayer organic absorbates on a metal surface with the model CuPc/Cu(111) system. Post-deposition annealing bonds CuPc molecules into dendrite-like clusters that are often mobile at room temperature. Substrate surface defects create energetic barriers that prevent CuPc cluster motion on the metal surface. This phenomenon was unveiled by the motion of small clusters that show rigid-body diffusion solely in the available space in between defects. When clusters are sufficiently surrounded by defects, they become completely pinned in place and become immobilized.

KEYWORDS: surface defects, on-surface synthesis, CuPc, Cu(111), scanning tunneling microscopy, density functional theory

I. Introduction

Synthesis of low dimensional materials from molecular building blocks is a rich and promising area of molecular nanotechnology [1,2]. A common route for material synthesis involves facilitating covalent bonding between precursor molecules on an atomically flat substrate through an annealing treatment. The substrate, often a transition metal, assists in the reaction by limiting the adsorbed molecules to the 2D surface and may act as a catalyst by providing adatoms for reaction intermediates [3-5]. One practical challenge with these coupled self-assemblies lies in

determining the fundamental mechanisms and interactions that are important in the design of the formed polymer or oligomer. Discovering what controls these factors may lead to new physical and chemical insights in low dimensional systems. For instance, it has been demonstrated that polymer/oligomer morphology is greatly affected by changes in adsorbate surface mobility [6,7], temperature-dependent bonding mechanisms [8,9], and substrate temperature during precursor deposition [10].

Point defects on the substrate surface are overlooked in this synthesis process. While experimental preparation techniques have advanced to generate nearly ideal substrates, surface defects are almost always unavoidable. These defects may physically and chemically interfere with precursors and modify reaction mechanisms. Thus, these defects merit a careful investigation. In this paper, we investigate the role of surface defects through the study of annealed sub-monolayer (ML) copper-phthalocyanine (CuPc) on Cu(111) with scanning tunneling microscopy (STM) and density functional theory (DFT) stimulations.

CuPc/Cu(111) is a model 2D π -conjugated molecule-metal system. Such systems form a variety of 2D structures [11,12] and have applications ranging from catalysis [13], molecular spintronics [14,15], and organic electronic devices [16,17]. Specifically, the CuPc/Cu(111) system has been extensively characterized across many techniques from sub-ML to multi-layer coverage across a large temperature range [18-30]. Room temperature (RT) STM experiments show that CuPc is highly mobile on noble metal (111) surfaces under 1 ML [21,28,29,31]. The STM tip measures the time averaged motion of CuPc across the surface as a diffusive background feature, as well as interference patterns from CuPc scattering around surface defects and step edge. Similar metal-phthalocyanine (MePc)/metal systems [32-34] show evidence of C-C bond formation after annealing, however bond formation through annealing has yet to be investigated on CuPc/Cu(111).

We find that annealing CuPc on Cu(111) yields dendrite-like clusters as a result of a dehydrogenation reaction that creates biphenyl links between molecules. CuPc appears to become immobilized after forming clusters, however, many smaller clusters diffuse and rotate on the Cu(111) terraces. Experimental observations and theoretical calculations demonstrate that clusters are immobilized by the energetic barriers created around surface defects that prevent CuPc diffusion over such defects. This reveals that the stochastic nature of surface defects can severely constrain the cluster's surface mobility. Considering the significance of CuPc/Cu(111) as a prototypical system, we believe that these findings greatly add to the fundamental understanding

of on-surface synthesis and may promote further studies of phthalocyanines, porphyrins, and other 2D π -conjugated molecules.

II. Experimental and Theoretical Details

Experiments were carried out in an RT ultra-high vacuum (UHV) STM chamber with a base pressure $\sim 3.0 \times 10^{-10}$ Torr. The Cu(111) substrate was cleaned by alternating cycles of Ar⁺ sputtering at 0.85 KeV and annealing at ~ 773 K. Sputtering cycles lasted 20 minutes and annealing cycles varied from 10 to 50 minutes. CuPc was evaporated from a sublimated purified CuPc powder inside a direct-current heated quartz Knudsen cell. Current controlled deposition was monitored by an in-situ quartz crystal microbalance (QCM) and the deposition rate was measured to be ~ 0.15 ML/min. Post-deposition annealing occurred at ~ 573 K via a ceramic radiative heater placed on the back of the Cu(111) sample plate. This temperature was slightly higher than previously reported experiments on CuPc/Cu(111) that did not show bonding [22,23]. Post-deposition annealing times varied from 15 to 30 minutes. Images were collected with Pt-Ir tips in the constant current mode and post-processed with WSxM [35].

DFT simulations were performed using VASP [36] with projector augmented-wave potentials [37,38], GGA-BPE functionals [39], and DFT-D3 and Becke-Jonson damping for van der Waals corrections [40,41]. Simulation details included a kinetic energy cut off of 500 eV and gamma point sampling (which is adequate due to the large super cells described below). Self-consistent calculations utilized a threshold of 10^{-4} eV/Å for force convergence and a threshold of 10^{-5} eV for total energy convergence. Further simulations details are included in ref. [42]. Four different Cu(111) slabs were created for DFT simulations. A 4 layer slab (10×10 Cu atoms) was used to model single CuPc adsorption and CuPc adsorption near a sulfur impurity. A 3 layer slab (10×15 Cu atoms) was used to model CuPc-CuPc bonding and non-bonding interactions. A 4 layer slab (34 Cu atoms per layer) was created to model the adsorption geometry of 1 ML of CuPc on Cu(111) (structure taken from ref. [27]). A 370 atom Cu(111) step edge slab was created to model CuPc adsorption near step edges of the Cu(111) surface. This slab was a modified version of the $4 \times 10 \times 10$ Cu atom slab and featured a step edge along a close packed direction. STM simulations followed the Tersoff-Hamann theory [43].

III. Results and Discussion

An example of covalently bonded CuPc clusters created at 0.25 ML is shown in Fig. 1(a). These dendrite-like clusters are heavily branched, often extend across entire Cu(111) terraces, and are on the order of 50 CuPc molecules in size when not limited by step edges. Clusters are primarily formed out of two different intermolecular bonding orientations; a parallel orientation, shown in Fig. 1(b), where bonding lobes of the CuPc lie along parallel lines and an angular orientation, shown in Fig. 1(c), where bonding lobes lie 120 degrees apart. DFT simulations of these bonding arrangements are shown in Fig. 1(d) to 1(g) and they strongly support the formation of C-C bonds. STM simulations and Cu-Cu distances from DFT calculations match the experimental observations well. Additionally, the reduced C_{2v} symmetry of the CuPc molecule is clearly visible. This symmetry is induced through interaction of the Cu(111) surface and can be observed as the bright and dark lobes seen on the CuPc molecules. C_{2v} symmetries of MePc molecules are consistent with previous observations across (111) metal surfaces [19,30,44]. Prior theoretical calculations [45,46] have shown that brighter lobes align with close packed directions of the substrate. While the bonding lobes in Fig. 1(b) and the non-bonding lobes in Fig. 1(c) are slightly brighter, the opposite cases were also observed, albeit less frequently [42]. This suggests that CuPc orientation on the substrate has a negligible influence on the type of bond formed.

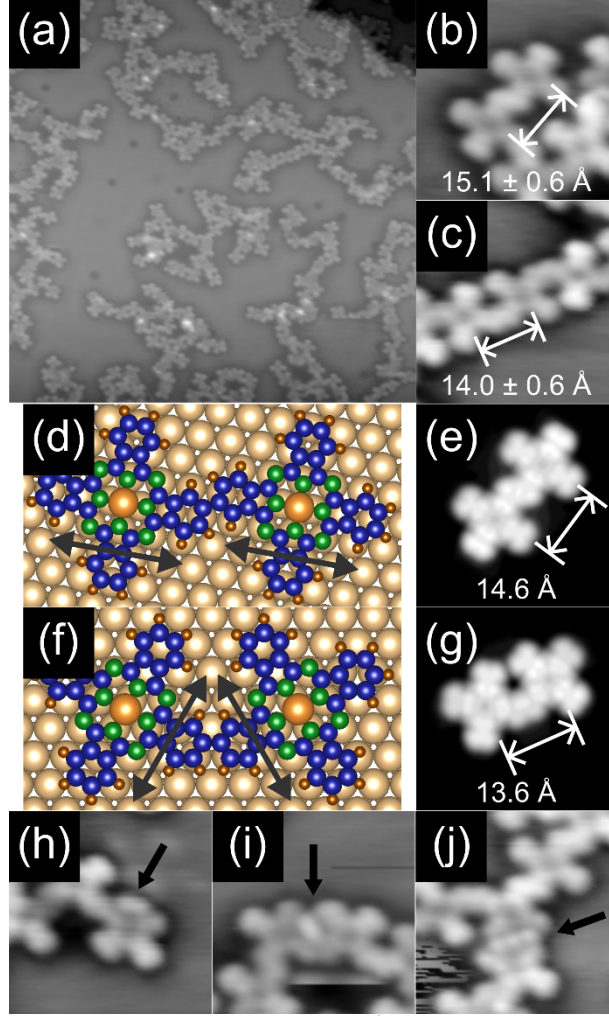


FIG. 1. (a) Annealed 0.25 ML CuPc on Cu(111) ($500 \times 500 \text{ \AA}^2$). (b)-(c) Specific parallel and angular bonding orientations ($50 \times 50 \text{ \AA}^2$). (d)-(e) Atomic model and STM simulation of parallel bonding. (f)-(g) Atomic model and STM simulation of angular bonding. (h)-(j) Different CuPc-Cu adatom coordination structures ($50 \times 50 \text{ \AA}^2$). STM simulations at +0.9 V. Imaged +0.9 V and 0.5 nA.

Each isoindole lobe of the CuPc molecule features two bonding sites on the peripheral carbon atoms, however steric hindrance limits each lobe to one bond only. These bonding orientations match the structures observed previously on CuPc/Ag(111) [32], FePc/Cu(111) [33], and ZnPc/Cu(100) [34] (parallel bonding only) which suggests that the formation of the biphenyl link is minimally dependent on the choice of metal center and metal substrate. The biphenyl link bears a similarity to, but is different from, the bonding observed with annealed octaethyl-tetra-azaporphyrin (OETAP) on Au(111) [10]. Post-deposition annealing transforms OETAP into phthalocyanine which become bonded together through naphthalene links. These naphthalene links place molecules closer together than biphenyl links and are inconsistent with our observations. Additionally, the benzene terminated lobes of CuPc are structurally and chemically

different from the ethylene terminated lobes of OETAP which are required for that specific reaction. Despite different bonding schemes, both surfaces show similar dendrite-like clusters. Interestingly, the Au(111) surface reconstruction appears to spatially confine the annealed OETAP clusters which preferentially grow in the FCC regions of the herringbone structure. On Cu(111) the CuPc clusters show no preferred morphology and tend to grow in all directions.

In rare instances, CuPc-Cu adatom coordination was observed. Several seemingly hierarchical structures were formed as depicted in Fig. 1(h)-1(j). The lobes near Cu adatoms are adsorbed closer to the surface as they appear darker in STM images. It is likely that CuPc are stabilized by this interaction, similar to how single Ag adatoms have been shown to stabilize CuPc on Ag(100) [47].

Different CuPc coverages were studied to measure changes in cluster size upon annealing. At 0.15 ML, many smaller clusters were observed (compared to 0.25 ML) that were spread evenly over the surface. The smallest resolvable cluster contained three CuPc molecules. Surprisingly, repeated STM scans (~ 10 minutes per image) revealed rigid-body motion by a fraction of the clusters, including diffusion and rotations, as shown in Fig. 2. Cluster diffusion between several specific locations was frequently observed. Sometimes clusters moved several nanometers in between scans. Rotations, which were rarely observed, featured stable positions on the Cu surface that were roughly 60 degrees apart. This suggests that rotating clusters were aligning with close packed directions. When mobile clusters interacted with immobile clusters, as in Fig. 2(f) to 2(h), the CuPc-CuPc distances from the nearest interacting CuPc molecules were sufficiently large to conclude that they were not bonding to each other. Clusters bonded to CuPc at step edges, as well as clusters with CuPc-Cu adatom coordinate were observed to be immobile.

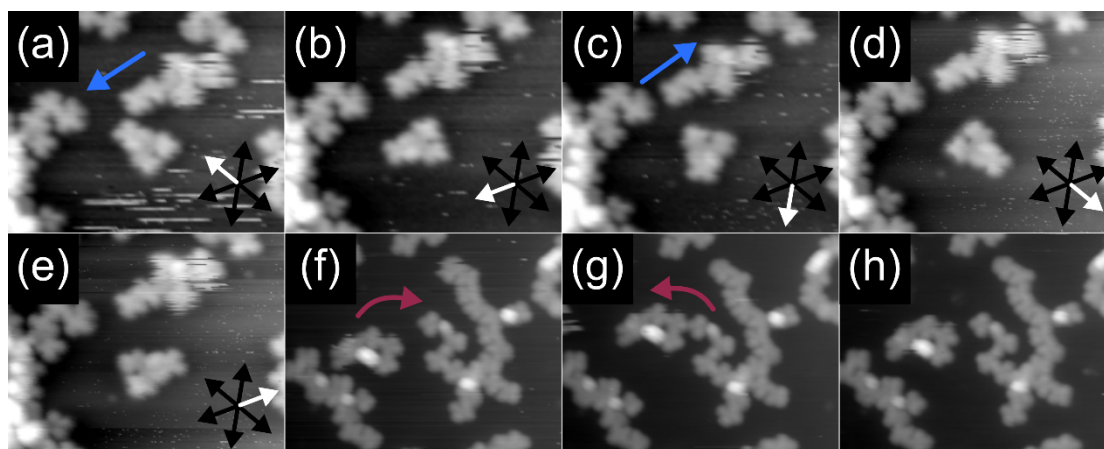


FIG. 2. 0.15 ML CuPc on Cu(111) with post-deposition annealing. (a)-(e) Rotational configurations of a CuPc cluster (-1.0 V, 0.5 nA, 200×160 Å²). Diffusion back and forth between different orientations was observed across 17 sequential images recorded over a 3.5-hour period. Translations by another cluster are

also indicated by blue arrows. (f)-(h) Interaction between different CuPc clusters across three sequential scans (-1.1 V, 0.5 nA, 250×200 Å²).

The observed cluster motion was varied and complex. Mobile clusters were sometimes well-resolved and other times noisy from scan to scan. Evidently, mobile clusters could be motionless or in motion while the STM tip was scanning directly above the cluster. In general, smaller clusters were more likely to be mobile. One possible explanation is that the larger clusters diffuse at slower rates due to their size and eventually, at a threshold size, become too large to move. However, this does not explain why some very small clusters (< 5 CuPc) were immobile yet many larger clusters (up to ~20 CuPc) were mobile. Possibilities of tip induced effects, such as a chemisorption mechanism [26,48-50] or local electric fields [51] are not likely as motion was observed at both scanning biases and no voltage pulses were applied from the tip.

It is already understood that CuPc molecules on clean Cu(111) are highly mobile at RT at sub ML coverages. CuPc will diffuse on terraces and adsorb at step edges. An ordered 2D CuPc phase only becomes apparent to STM as the coverage reaches 1 ML and the second layer of CuPc only begins to form once the first ML is completed [27].

To further understand cluster mobility, additional CuPc can be deposited on a surface with CuPc clusters without subsequent annealing. Thus, differences in mobility between clusters and single molecules is easily distinguishable in the same STM scan. Fig. 3 displays the annealed 0.15 ML CuPc surface before and after adding an additional 0.15 ML CuPc without annealing. In Fig. 3(a) noisy streaks, which are topographically the same height as the immobile clusters, are indicated with white arrows. The diffuse background created by highly mobile CuPc in Fig. 3(b) sits at a lower topographic height and is considerably different than the noisy streaks (see refs. [31,52] for more information). We attribute the noisy streaks to CuPc clusters – possibly bonded CuPc pairs – that were moving too quickly to be fully resolved by the tip. These streaks appear brighter than the diffusive background because they are diffusing more slowly than individual CuPc molecules and therefore spend a larger amount of time under the STM tip.

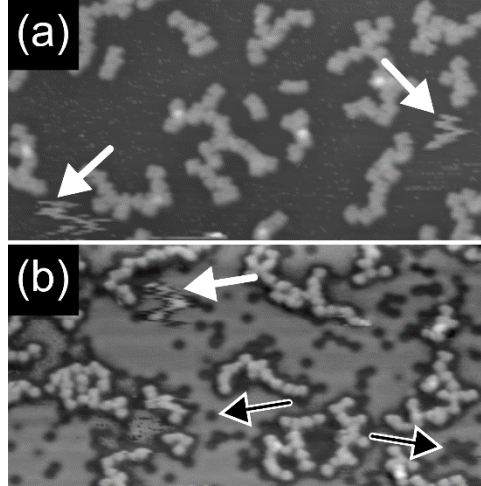


FIG. 3. Addition of 0.15 ML CuPc without annealing. (a) STM scan of annealed CuPc before additional deposition (-2.0 V, 0.1 nA, $600 \times 350 \text{ \AA}^2$). (b) STM scan after additional deposition of CuPc (-1.2 V, 0.5 nA, $600 \times 350 \text{ \AA}^2$).

Single CuPc molecules also scatter off CuPc clusters. Regions devoid of the diffusive background around surface defects are also found around clusters. A few surface defects are indicated in Fig. 3(b) with black arrows. Regions between defects that CuPc molecules are physically incapable of occupying show no diffusive background, giving the appearance of extended defect structures (more details in ref. [42]).

A series of DFT simulations provides insights into the behavior of sub -ML CuPc on Cu(111) by measuring the change in CuPc adsorption energy across a variety of CuPc/substrate interactions. Fig. 4 displays the clear trend that CuPc is further stabilized by increasing the interaction with substrate atoms and is less stabilized upon increasing CuPc-CuPc interaction. When CuPc interacts at or near a step edge the adsorption energy is $\sim 1 \text{ eV}$ more stable. Isolated CuPc and monolayer CuPc occupy a range of roughly 0.48 eV due to the different possible positions of the molecules on the Cu(111) surface [42]. The adsorption energy begins to quickly drop as CuPc lobes are removed from the Cu(111) surface and forced to interact with other CuPc. CuPc in the 2nd ML are $\sim 2.65 \text{ eV}$ less stable.

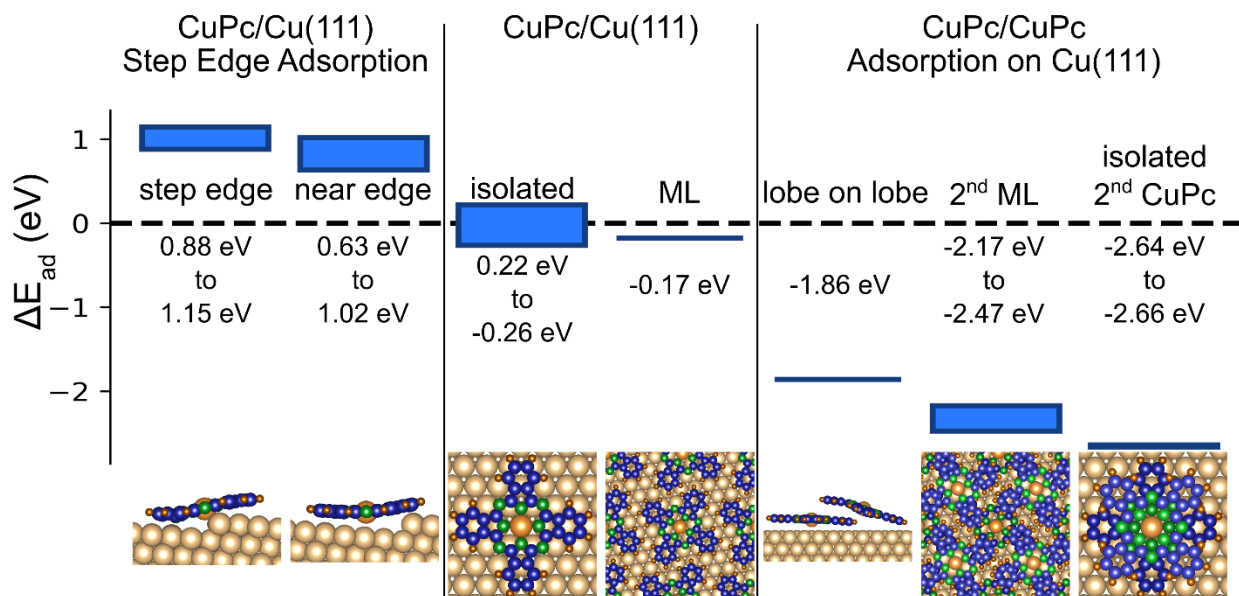


FIG. 4. Relative stability of CuPc across various interaction schemes. CuPc adsorption on Cu(111) is used as the reference energy. The energy ranges come from taking the range of adsorption energies from several different geometries (details in ref. [42]). Positive energies are more stable.

These energies provide results consistent with the experimental observations. CuPc deposited onto Cu(111) at RT can further increase its stability by adsorbing at step edges. The ~ 1 eV increase in stability is larger than the thermal energy of CuPc as the molecules do not desorb from the step edges. When CuPc is deposited onto the post-annealed surface (with immobile CuPc clusters) no single CuPc molecules remain on top of clusters. If CuPc were to land on top of an immobile cluster, the CuPc would increase its energetic stability by transitioning off the cluster and onto the available Cu(111) surface.

Repeated STM scans of the cluster plus single molecule surface, shown in Fig. 5, clearly show that the highlighted surface defects hinder cluster mobility. The clusters surrounded by defects outlined in white and red move within their defect free region from scan to scan and never move over any defects. The cluster surrounded by defects outlined in blue moves very quickly inside its defect free region, then appears to become freed from that space in Fig. 5(b) as the noisy streaks indicative of the cluster disappears. It is likely that this cluster squeezed through the two leftmost highlighted defects as a characteristic noisy streak is observed to the left of the defects in Fig. 5(c).

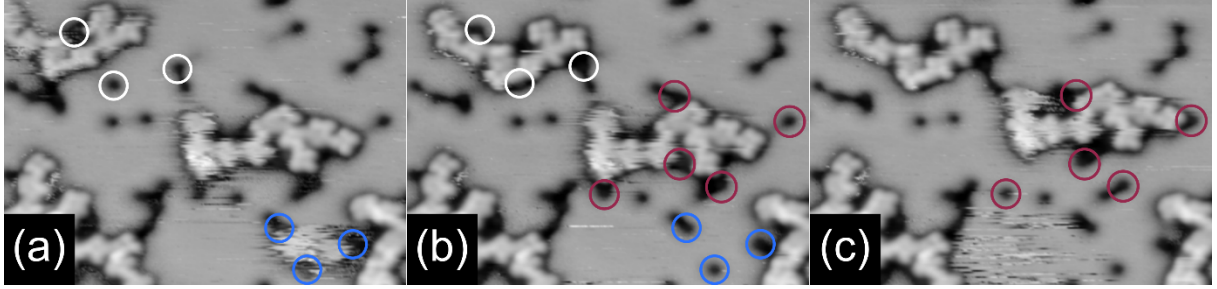


FIG. 5. (a)-(c) Sequential scans that track mobile cluster movement. From panel (a) to (b) the topmost cluster moves until it is pinned by surface defects outlined in white. Another cluster, enclosed by defects outlined with blue, disappears in panel (b). From panel (b) to (c) motion of another cluster is hindered by defects outlined in red. All imaged at -1.0 V, 0.4 nA, $300 \times 180 \text{ \AA}^2$.

Surface defects acting as pinning sites for CuPc cluster motion provide an adequate explanation for the observed cluster motion. Very small clusters should almost always be mobile as they would be able to move in between most surface defects. If a cluster is surrounded by a few defects, such as those surrounded by highlighted defects in Fig. 5, it is possible that motion is restricted to a small area. If surrounded by enough surface defects the entire cluster would become immobilized. As the cluster size increases, it is more likely to be surrounded by enough surface defects to immobilize the cluster. Due to the stochastic nature of surface defects, it is possible that some larger clusters remain mobile while smaller clusters are immobile. It is also likely that larger clusters diffuse more slowly on the surface. However, surface defects, step edges, and Cu adatom coordination appear to be the most important factors responsible for cluster immobilization. The importance of surface defects revealed here may have significant consequences across a large variety of molecule/metal systems. This mechanism may explain the mobility (and lack of mobility) in other cases of rigid-body diffusion of bonded molecules [10,53], especially those where the mobility of the molecular cluster largely deviates from that of individual molecules.

Auger spectroscopy on Cu(111) single crystals prepared in a similar manner to our samples has revealed that sulfur is likely the primary surface contaminant [54]. Annealing cycles used in sample preparation enables sulfur to diffuse from the bulk to the surface. Fig. 6(a) and 6(b) display typical STM images of surface defects on Cu(111) before and after a tip change. Their observed morphology is characteristic of STM images of isolated sulfur deposited on Cu(001) [55], and not like the Cu_2S_3 complexes or reconstructed steps observed with sulfur deposited on Cu(111) [56,57]. Given the appearance of the defects in our data, we assume that isolated sulfur atoms are the primary surface defect responsible for hindering cluster motion.

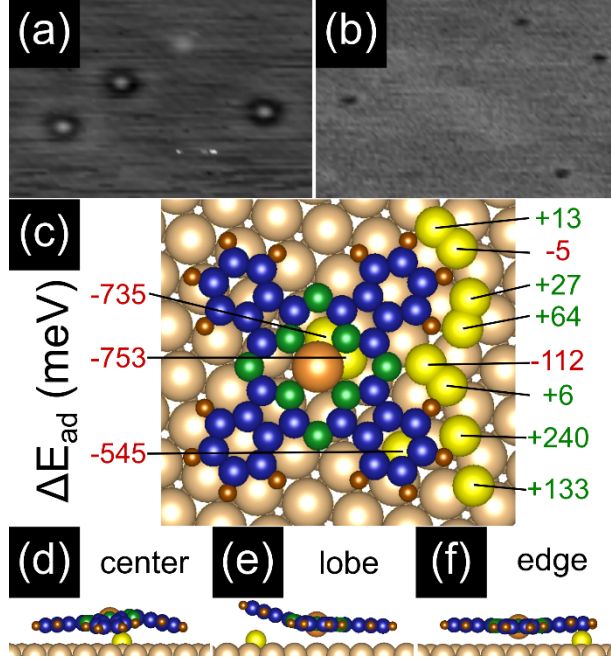


FIG. 6. (a)-(b) Surface defects on Cu(111) before and after a tip change (-1,2 V, 0.2 nA, $120 \times 80 \text{ \AA}^2$) (c) Relative adsorption energies of CuPc near and on top of S defects. (d)-(f) Three relaxed geometries of CuPc by S on Cu(111).

DFT simulations of this type of defect reveal how cluster motion is hindered. Eleven different FCC and HCP sites were populated with a sulfur atom either underneath or beside an isolated CuPc molecule. The locations of these sites and the changes in adsorption energy, ΔE_{ad} , are shown in Fig. 6(c). Negative values indicate a less favorable adsorption configuration. Fig. 6(d) to 6(f) display the relaxed geometry of a few cases. Sulfur placed near the edge of the lobes show a slight increase in adsorption energy. However, these small changes are comparable to changes in energy as CuPc moves across the Cu(111) surface and theoretical activation barriers for CoPc diffusion on Ag(100) [58] and various MePc on Au(111) [59]. Thus, sulfur near CuPc minimally affects the molecule. Sulfur underneath CuPc however, is not favorable as it interferes with the adsorbate-substrate interaction. The unfavorable adsorption of CuPc on top of sulfur demonstrates that CuPc molecules (and clusters) experience a significant energetic barrier as they try to move over a surface defect. In the case of single molecules this produces scattering patterns [26]. In the case of clusters this hinders motion in the xy-plane and can effectively trap clusters.

IV. Conclusion

A new mechanism is presented whereby molecular clusters are immobilized by substrate surface defects. Dendrite-like CuPc clusters reveal complex rigid-body mobility (and immobility) on the Cu(111) surface that is, to a first-order approximation, cluster size dependent but also subject to

stochastic randomness from the distribution of substrate surface defects. Surface defect pinning, in combination with substrate step edges, native adatoms coordination, and size dependent diffusion constants provide a complete picture of how and why mobile precursor molecules may combine into immobile polymers and oligomers.

V. Acknowledgements

This research was possible through the support provided by Natural Sciences and Engineering Research Council of Canada (NSERC), Hart Professorship, and the University of Toronto. Computations were conducted through the Compute Canada facilities, namely the Niagara cluster. The authors declare no competing financial interests.

References

- [1] G. M. Whitesides, J. P. Mathias, and C. T. Seto, *Science* **254**, 1312 (1991).
- [2] J. V. Barth, G. Costantini, and K. Kern, *Nature* **437**, 671 (2005).
- [3] L. Bartels, *Nat. Chem.* **22**, 87 (2010).
- [4] G. Franc and A. Gourdon, *Phys. Chem. Chem. Phys.* **13**, 14283 (2011).
- [5] S. Clair and D. G. de Oteyza, *Chem. Rev.* **119**, 4717 (2019).
- [6] M. Bieri *et al.*, *J. Am. Chem. Soc.* **132**, 16669 (2010).
- [7] A. L. Pinardi *et al.*, *ACS Nano* **7**, 3676 (2013).
- [8] L. Lafferentz, V. Eberhardt, C. Dri, C. Africh, G. Comelli, F. Esch, S. Hecht, and L. Grill, *Nat. Chem.* **4**, 215 (2012).
- [9] Q. Li *et al.*, *J. Am. Chem. Soc.* **138**, 2809 (2016).
- [10] B. Cirera *et al.*, *Nat. Comms.* **7**, 11002 (2016).
- [11] J. M. Gottfried, *Sur. Sci. Rep.* **70**, 259 (2015).
- [12] W. Auwärter, D. Écija, F. Klappenberger, and J. V. Barth, *Nat. Chem.* **7**, 105 (2015).
- [13] A. B. Sorokin, *Chem. Rev.* **113**, 8152 (2013).
- [14] S. Sanvito, *Chem. Soc. Rev.* **40**, 3336 (2011).
- [15] R. Geng, H. M. Luong, T. T. Daugherty, L. Hornak, and T. D. Nguyen, *J. Sci. Adv. Mater. Dev.* **1**, 256 (2016).
- [16] G. Bottari, G. de la Torre, D. M. Guldi, and T. Torres, *Chem. Rev.* **110**, 6768 (2010).
- [17] O. A. Melville, B. H. Lessard, and T. P. Bender, *ACS Appl. Mater. Interfaces* **7**, 13105 (2015).
- [18] J. C. Buchholz and G. A. Somorjai, *J. Chem. Phys.* **66**, 573 (1977).
- [19] H. Karacuban, M. Lange, J. Schaffert, O. Weingart, T. Wagner, and R. Möller, *Surf. Sci.* **603**, L39 (2009).
- [20] D. G. de Oteyza *et al.*, *J. Chem. Phys.* **133**, 214703 (2010).
- [21] I. Kröger, B. Stadtmüller, C. Wagner, C. Weiss, R. Temriov, F. S. Tautz, and C. Kumpf, *J. Chem. Phys.* **135**, 234703 (2011).
- [22] B. Stadtmüller, I. Kröger, F. Reinert, and C. Kumpf, *Phys. Rev. B* **83**, 085416 (2011).
- [23] I. Kröger, B. Stadtmüller, C. Kleimann, P. Rajput, and C. Kumpf, *Phys. Rev. B* **83**, 195414 (2011).
- [24] J. Schaffert, M. C. Cottin, A. Sonntag, C. A. Bobisch, R. Möller, J.-P. Gauyacq, and N. Lorente, *Phys. Rev. B* **88**, 075410 (2013).
- [25] J. Schaffert, M. C. Cottin, A. Sonntag, H. Karacuban, C. A. Bobisch, N. Lorente, J.-P. Gauyacq, and R. Möller, *Nat. Mater* **12**, 223 (2013).

- [26] T. J. Z. Stock and J. Nogami, Appl. Phys. Lett. **104**, 071601 (2014).
- [27] T. J. Z. Stock and J. Nogami, Surf. Sci. **637-638**, 132 (2015).
- [28] T. J. Z. Stock, University of Toronto, 2015.
- [29] M. Mehdizadeh, University of Toronto, 2017.
- [30] S. Fremy-Koch, A. Sadeghi, R. é. m. Pawlak, S. Kawai, A. Baratoff, S. Goedecker, E. Meyer, and T. Glatzel, Phys. Rev. B **100**, 155427 (2019).
- [31] G. Antczak, K. Boom, and K. Morgenstern, J. Phys. Chem. C **121**, 542 (2017).
- [32] K. Manandhar, T. Ellis, K. T. Park, T. Cai, Z. Song, and J. Hrbek, Surf. Sci. **601**, 3623 (2007).
- [33] O. Snezhkova *et al.*, J. Chem. Phys. **144**, 094702 (2016).
- [34] F. Chen *et al.*, Appl. Phys. Lett. **100**, 081602 (2012).
- [35] I. Horcas, R. Fernández, J. M. Gómez-Rodríguez, J. Colchero, J. Gómez-Herrero, and A. M. Baro, Rev. Sci. Instrum. **78**, 013705 (2007).
- [36] G. Kresse and F. J., Phys. Rev. B **54**, 11169 (1996).
- [37] P. E. Blöchl, Phys. Rev. B **50**, 17953 (1994).
- [38] G. Kresse and D. Joubert, Phys. Rev. B **59**, 1758 (1999).
- [39] J. P. Perdew, K. Burke, and M. Ernzerhof, Phys. Rev. Lett. **77**, 3865 (1996).
- [40] S. Grimme, J. Antony, S. Ehrlich, and H. Krieg, J. Chem. Phys. **132**, 154104 (2010).
- [41] S. Grimme, S. Ehrlich, and L. Goerigk, J. Comp. Chem. **32**, 1456 (2011).
- [42] See Supplemental Material at [*URL will be inserted by publisher*] for more information on CuPc clusters, cluster statics, and DFT simulations.
- [43] J. Tersoff and D. R. Hamann, Phys. Rev. B **31**, 805 (1985).
- [44] S.-H. Chang, S. Kuck, J. Brede, L. Lichtenstein, G. Hoffmann, and R. Wiesendanger, Phys. Rev. B **78**, 233409 (2008).
- [45] J. D. Baran and J. A. Larsson, J. Phys. Chem. C **117**, 23887–23898 (2013).
- [46] D. Lüftner, M. Milko, S. Huppmann, M. Scholz, N. Ngyuen, M. Wießner, A. Schöll, F. Reinert, and P. Puschniga, J ELECTRON SPECTROSC **195**, 293 (2014).
- [47] G. Antczak, W. Kamiński, and K. Morgenstern, J. Phys. Chem. C **119**, 1442 (2014).
- [48] Y. C. Jeong, S. Y. Song, K. Y., O. Y., K. J., and S. J., J. Phys. Chem. C **119**, 27721 (2015).
- [49] A. Zhao *et al.*, Science **309**, 1542 (2005).
- [50] L. Chen, H. Li, and A. T. S. Wee, ACS Nano **3**, 3684 (2009).
- [51] K. Nagaoka, S. Yaginuma, and T. Nakayama, Jap. J. App. Phys. **57**, 020301 (2018).
- [52] P. Matvija, F. Rozbořil, P. Sobotík, I. Ošťádal, and P. Kocán, J. Phys. Chem. Lett. **8**, 4268 (2017).
- [53] M. In't Veld, P. Iavicoli, S. Haq, D. B. Amabilino, and R. Raval, Chem. Commun., 1536 (2008).
- [54] B. J. Hinch, J. W. M. Frenken, G. Zhang, and J. P. Toennies, Surf. Sci. **259**, 288 (1991).
- [55] H. Walen, D.-J. Liu, J. Oh, H. J. Yang, P. M. Spurgeon, Y. Kim, and P. A. Thiel, J. Phys. Chem. B **122**, 963 (2017).
- [56] H. Walen, D.-J. Liu, J. Oh, H. Lim, J. W. Evans, C. M. Aikens, Y. Kim, and P. A. Thiel, Phys. Rev. B **91**, 045426 (2015).
- [57] H. Walen, D.-J. Liu, J. Oh, H. Lim, J. W. Evans, Y. Kim, and P. A. Thiel, J. Chem. Phys. **142**, 194711 (2015).
- [58] G. y. Antczak, W. Kamiński, A. Sabik, C. Zaum, and K. Morgenstern, J. Am. Chem. Soc. **137**, 14920 (2015).
- [59] L. Buimaga-Iarinca and C. Morari, Sci. Rep. **8**, 12728 (2018).